New Insights into the Heme Cavity Structure of Catalase-Peroxidase: A Spectroscopic Approach to the Recombinant *Synechocystis* Enzyme and Selected Distal Cavity Mutants†

Hendrik A. Heering,‡ Chiara Indiani,‡ Günther Regelsberger,§ Christa Jakopitsch,§ Christian Obinger,§ and Giulietta Smulevich*,‡

Dipartimento di Chimica, Universita' di Firenze, Polo Scientifico, Via della Lastruccia 3, I-50019 Sesto Fiorentino (FI), Italy, and Institute of Chemistry, University of Agricultural Sciences, Muthgasse 18, A-1190 Vienna, Austria

Received February 28, 2002; Revised Manuscript Received May 2, 2002

ABSTRACT: Catalase-peroxidases (KatGs) are heme peroxidases with homology to yeast cytochrome *c* peroxidase (CCP) and plant ascorbate peroxidases (APXs). KatGs exhibit a peroxidase activity of broad specificity and a high catalase activity, which strongly depends on the presence of a distal Trp as part of the conserved amino acid triad Arg-Trp-His. By contrast, both CCP and APX do not have a substantial catalase activity despite the presence of the same triad. Thus, to elucidate structure−function relationships of catalase-peroxidases (for which no crystal structure is available at the moment), we performed UV−Vis and resonance Raman studies of recombinant wild-type KatG from the cyanobacterium *Synechocystis* PCC 6803 and the distal side variants (His123→Gln, Glu; Arg119→Ala, Asn; Trp122→Phe, Ala). The distal cavity of KatG is very similar to that of the other class I peroxidases. A H-bond network involving water molecules and the distal Trp, Arg, and His is present, which connects the distal and proximal sides of the heme pocket. However, distal mutation not only affects the heme Fe coordination state and perturbs the proximal Fe−Im bond, as previously observed for other peroxidases, but also alters the stability of the heme architecture. The charge of the distal residues appears particularly important for maintaining the heme architecture. Moreover, the Trp plays a significant role in the distal H-bonding, much more pronounced than in CCP. The relevance of these findings for the catalase activity of KatG is discussed in light of the complete loss of catalase activity in the distal Trp mutants.

In 1979 a new class of bacterial enzymes, the catalase-peroxidases (KatGs),[1] was identified. KatGs have been isolated from a variety of different prokaryotes (archaebacteria and eubacteria) and fungi. Although these enzymes show high catalase activity, they have little sequence homology with typical heme-containing monofunctional catalases. On the other hand, they have homology with yeast cytochrome *c* peroxidase (CCP) and ascorbate peroxidase (APX). Thus, they have been recognized as part of class I of the peroxidase superfamily I (enzymes from plants, fungi, and bacteria) (*1*). Hence, KatGs are the only peroxidases known so far which have both catalase activity comparable with catalases as well as typical peroxidase activity with broad specificity.

Although the overexpression of KatG from several species has been reported (*2*−*7*), only a few mechanistic studies have been performed, and the structural basis for the catalase activity is still unclear. The three-dimensional structures of CCP and APX are known (*8*, *9*) and show highly conserved amino acid residues at the active site. No structural data are available from catalase-peroxidases, but both physical characterization and sequence analyses (*10*, *11*) unequivocally indicate that a histidine residue is the proximal ligand of heme iron. As for APX and CCP, the proximal histidine should have an imidazolate character because its δ-nitrogen could be H-bonded to a conserved aspartate residue. In APX and CCP, the latter is H-bonded to a tryptophan residue which is also conserved in KatG proteins. On the distal side, the high-resolution crystal structures of both CCP and APX indicate the presence of the triad Arg-Trp-His as well as a H-bond from the δ-nitrogen of the distal His to a near-surface asparagine. Sequence alignments suggest the presence of these residues also in the distal pocket of catalase-peroxidases

† This work was supported by grants from the Italian Consiglio Nazionale delle Ricerche (CNR) and the Ministry of Education, Universities, and Research (MIUR) to G.S., and by the Austrian Science Funds FWF (Project P15417) to C.O. The authors acknowledge the COST Action D21 "Metallo Enzymes and Chemical Biomimetics" for supporting the exchange among the different laboratories.

* To whom correspondence should be addressed. Tel: +39 0554573083; Fax: +39 0554573077; E-mail: giulietta.smulevich@unifi.it.

‡ Universita' di Firenze.

§ University of Agricultural Sciences.

[1] Abbreviations: KatG, catalase-peroxidase; APX, ascorbate peroxidase; CCP, cytochrome *c* peroxidase; CCP(MI), cytochrome *c* peroxidase expressed in *E. coli* containing Met-Ile at the N-terminus; CIP, *Coprinus cinereus* peroxidase, expressed in *Aspergillus oryzae* (identical to ARP, *Arthromyces ramosus* peroxidase); HRPC, horseradish peroxidase isoenzyme C; HRPA2, horseradish peroxidase isoenzyme A2; LIP, lignin peroxidase; Mb, myoglobin; SBP, soybean peroxidase; WT, wild type; MES, (2-[N−Morpholino]ethane sulfonic acid); bicine, (*N*,*N*-bis[2-hydroxyethyl] glycine); CT1, long wavelength (>600 nm) porphyrin-to-metal charge transfer band; RR, resonance Raman; 5-c, five-coordinate; 6-c, six-coordinate; HS, high-spin; LS, low-spin; QS, quantum mechanically mixed-spin.

10.1021/bi025740u CCC: $22.00
Published on Web 06/26/2002

(*10*, *11*). Mutations on the distal side were recently produced in the catalase-peroxidases from *E. coli* (*12*), *Synechocystis* PCC 6803 (*13*, *14*), and *Mycobacterium tuberculosis* (*15*). Very similar results were obtained irrespective of the origin of the KatG mutated. Selected distal side mutations of KatG display drastically reduced catalase activity and modified peroxidase activity. In particular, the distal mutants W122F and W122A (*Synechocystis* numbering) completely lost their catalase activity but retained their peroxidase activity (*13*, *14*). These results prompt the following question: if this highly conserved triad, especially the distal Trp, is so important for the catalatic process in KatGs, why do CCP and APX, which contain the same invariant catalytic triad, not exhibit catalatic activity? In the absence of any crystal structure for a catalase-peroxidase, we have to rely on sequence analysis and spectroscopic data of class I peroxidases to answer this question and reveal possible structural homologies and/or differences.

To elucidate structure−function relationships of catalase-peroxidases, we performed UV−Vis and resonance Raman (RR) investigations of a recombinant catalase-peroxidase from the cyanobacterium *Synechocystis* PCC 6803 (overexpressed in *E. coli*) and of distal variants with mutations at the conserved amino acid triad Arg-Trp-His (R119A, R119N, W122F, W122A, H123Q, H123E). Evidence for a H-bond network is provided, which involves water molecules, Trp, His, and Arg residues and connects the distal and proximal sides of the heme pocket. A detailed spectroscopic characterization of the distal variants as well as a comparison of the results with those already existing for CCP and APX is presented which affords a better understanding of class I peroxidases in general and the bifunctional activity of KatGs in particular. The importance of the distal Trp in KatG oxidation of hydrogen peroxide to molecular oxygen becomes evident from its significant role in distal H-bonding which is demonstrated in this work.

MATERIALS AND METHODS

Mutagenesis, expression, purification of KatGs from *Synechocystis* PCC 6803, and spectrophotometric characterization of wild-type and mutant proteins were described previously (*13*). Sample proteins were prepared in 50 mM sodium phospate buffer at pH 7.0. The fluoride complexes were prepared by diluting concentrated protein in 0.5 M NaF buffered with 50 mM sodium citrate at pH 6.4. The WT fluoride complex at pH 5.7 was obtained by adding 0.1 M NaF (Merck) to the ferric protein dissolved in 50 mM sodium phosphate/citrate. The R119N mutant was titrated with NaF in sodium citrate at pH 5.5. The ferrous enzyme was obtained by adding a small volume (2−4 μL) of fresh sodium dithionite solution (10−20 g/L $Na_2S_2O_4 \cdot 2H_2O$) to a deoxygenated protein solution (30−40 μL) in 100 mM MES [2-(*N*-morpholino)ethanesulfonic acid]/100 mM citric acid buffer, pH 5.7−5.8; 100 mM KH_2PO_4/100 mM citric acid, pH 6.5; 50 mM sodium phosphate, pH 7.1 and 7.5; 50 mM bicine [*N*,*N*-bis(2-hydroxyethyl)glycine], pH 8.4; or 50 mM boric acid/50 mM glycine, pH 9.2. Deuterated ferrous KatG was prepared by lyophilizing a known volume of buffered protein solution (100 mM MES/100 mM citric acid, pH 5.8, or 100 mM sodium phosphate, pH 7.2) and redissolving in an equal amount of D_2O (pD 5.9 or 7.3, respectively). The protein was then reduced by sodium dithionite in D_2O as described above. Sample concentrations for RR experiments ranged from 25 to 80 μM. Electronic absorption spectra were measured in solutions containing between 5 and 90 μM protein.

Resonance Raman spectra were obtained by excitation with the 406.7 and 413.1 nm lines of a Kr^+ laser (Coherent, Innova 90/K) and by a 441.6 nm Hg/Cd laser (Liconix). The backscattered light from a slowly rotating NMR tube was collected and focused into a computer-controlled double monochromator (Jobin-Yvon HG 2S) equipped with a cooled photomultiplier (RCA C31034 A) and photon-counting electronics. The RR spectra were calibrated to an accuracy of ± 1 cm^{-1} for intense isolated bands, with indene as standard for the high-frequency region and with both indene and CCl_4 for the low-frequency region. To minimize local heating of the protein induced by the laser beam, the sample was cooled to approximately 15 °C by a gentle flow of N_2 gas passed through liquid N_2. Polarized spectra were obtained by inserting a polaroid analyzer between the sample and the entrance slit of the monochromator. The depolarization ratios, $\rho = I_\perp/I_{||}$, of the bands at 314 and 460 cm^{-1} of CCl_4 were measured to check the reliability of the polarization measurements. The values obtained, 0.73 and 0.00, respectively, compare well with the theoretical values of 0.75 and 0.00, respectively. To determine the H/D isotopic shifts of the ν(Fe−Im) stretching mode frequencies, the RR spectra of the ferrous KatG were deconvoluted by curve-fitting. Best fits were obtained using Lorentzian line shapes with a bandwidth of 19.0 cm^{-1}.

Electronic absorption spectra were recorded at room temperature (23 ± 1 °C) with a double-beam Cary 5 spectrophotometer both prior to and after RR measurements to check if sample degradation had occurred under the experimental conditions. No changes were observed.

RESULTS

Ferric Forms. Figure 1 compares the UV−Vis (panel A) and RR (panel B) spectra of CCP, KatG, and APX at neutral pH. In the electronic absorption spectrum of ferric KatG, both the Soret and the CT1 bands suggest the presence of a 5-c HS heme coexisting with a 6-c HS heme: the Soret band shows a shoulder at about 380 nm which is not very pronounced as in the case of a pure 5-c HS heme; moreover, the CT1 at 637 nm, characteristic of a 6-c HS, is broad at higher wavelength, indicating the presence of the 5-c HS heme (*16*). A small amount of 6-c LS heme can be inferred by the presence of a high background around 570−590 nm. On going from pH 7.0 to 5.7, the Soret band of KatG blue-shifts by 1 nm and decreases in intensity, while the shoulder at about 380 nm increases in intensity. Concomitantly, in the visible region, the CT1 band red-shifts (data not shown). These changes indicate an increase of the 5-c HS heme at the expense of 6-c HS heme. However, the titration of the ferric form between pH 5.0 and pH 11.1 shows that at pH lower than 6.6 the protein precipitates ~30 min after preparation, whereas it is stable between pH 7.0 and 9.5 and no changes are detected in the UV−Vis spectra. At higher pH, the protein loses the heme before any alkaline transition can be detected. The precipitation observed at pH below 6.6 coincides with the reported loss of activity (*13*), whereas

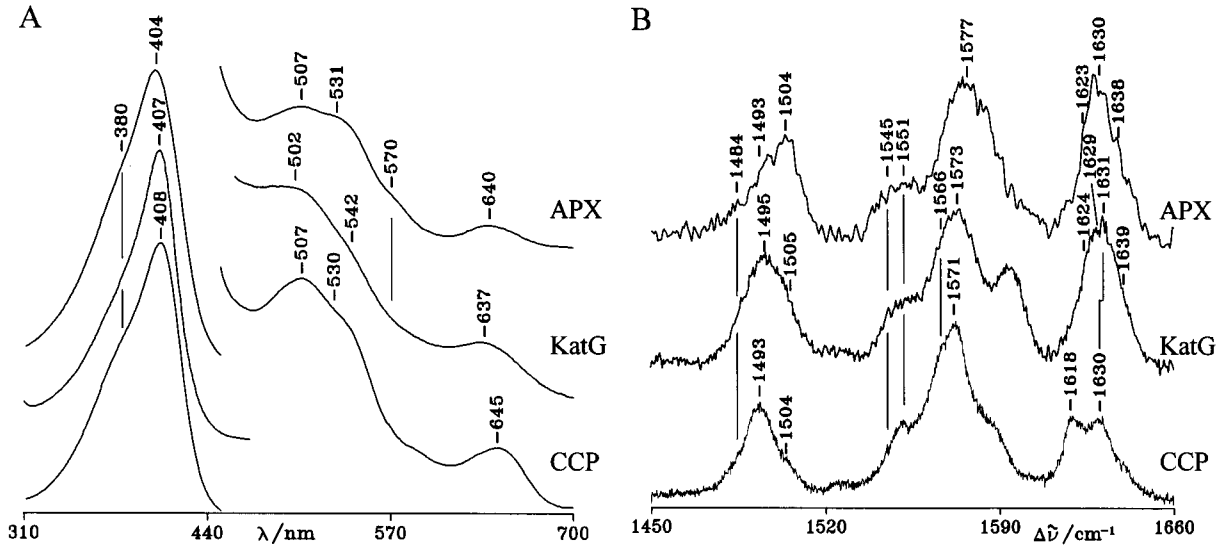

FIGURE 1: Panel A: electronic absorption spectra of ferric CCP (*18*), KatG, and APX (*18*) at neutral pH in phosphate buffer. The region between 450 and 700 nm has been expanded 8-fold. Panel B: corresponding RR spectra obtained with 413.1 nm [CCP and APX (*18*)] and 406.7 nm (KatG) excitation wavelength. Experimental conditions: 5 cm^{-1} resolution; (CCP) 20 s/0.2 cm^{-1} collection interval and 25 mW laser power at the sample; (KatG) 16 s/0.5 cm^{-1} collection interval and 15 mW laser power at the sample; (APX) 3 s/0.5 cm^{-1} collection interval and 7 mW laser power at the sample.

the decreased activity observed at pH higher than 7 must be due to a pH effect and not to protein denaturation since KatG is stable between pH 7.0 and 9.5.

The RR data at neutral pH confirm that ferric KatG is characterized by the presence of 5-c HS heme (ν_3 at 1495 cm^{-1}, ν_{11} at 1551 cm^{-1}, ν_2 at 1573 cm^{-1}, ν_{37} at 1594 cm^{-1}, ν_{10} at 1631 cm^{-1}) coexisting with a small amount of both 6-c HS (ν_3 at 1484 cm^{-1}, ν_{11} at 1545 cm^{-1}, ν_2 at 1566 cm^{-1}) and 6-c LS (ν_3 at 1505 cm^{-1}, ν_{10} at 1639 cm^{-1}) hemes (Figure 1B). Moreover, RR spectra in polarized light (data not shown) indicated that two bands at 1624 and 1629 cm^{-1} are polarized and, therefore, assigned to two ν(C═C) vinyl stretching modes.

The spectrum of KatG resembles that of CCP in terms of the percentage of the heme species present (*17*), whereas its similarities to APX are limited essentially to the vinyl ν(C═C) stretching mode frequencies (*18*). Two overlapping vinyl bands at 1618 cm^{-1} were observed for CCP, whereas APX showed the stretches at 1623 cm^{-1} (very weak) and at 1629 cm^{-1}. The KatG data suggest that the vinyl orientation is similar to that of APX, confirming the importance of the nature of the residues in the proximity of the vinyl groups. On the basis of RR spectra and local density functional calculations on mono- and divinylhemins, it has been proposed that when the protein matrix exerts no constraints on the vinyl groups, two distinct ν(C═C) stretching modes should be observed in their RR spectrum. One band, around 1620 cm^{-1}, is assigned to a nearly in-plane vinyl group and the other band, around 1630 cm^{-1}, to an out-of-plane vinyl group (*19*). X-ray structures of peroxidases show that the dihedral angle of vinyl 2 varies widely, whereas the angle of vinyl 4 varies in a smaller range. Accordingly, the RR ν(C═C) stretching frequencies vary from about 1618 to 1632 cm^{-1} (*20*). The X-ray structure of recombinant CCP (CCP-MI) (*21*) shows that both vinyls are oriented parallel to the pyrrole double bond due to the steric hindrance of the bulky Met172 residue in close proximity to vinyl 2 and both RR ν(C═C) are found to overlap at 1620 cm^{-1} (*22*). Met172 is

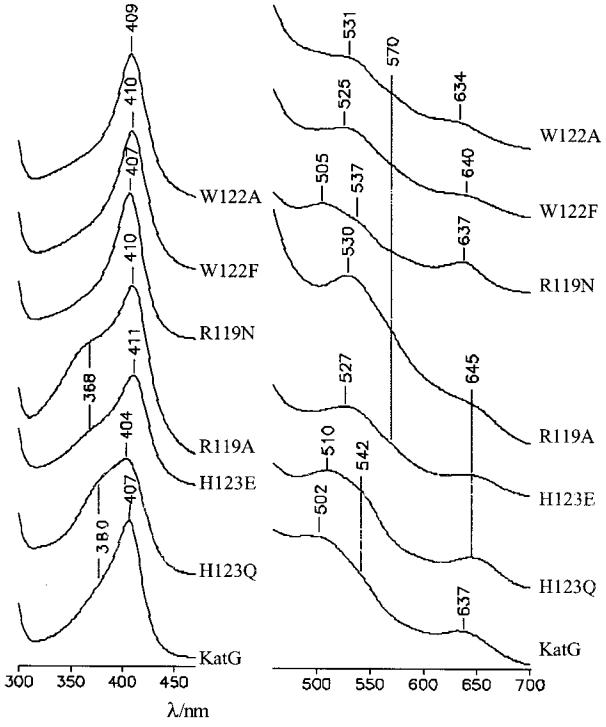

FIGURE 2: Electronic absorption spectra of ferric KatG and the distal mutants H123Q, H123E, R119A, R119N, W122F, and W122A at neutral pH in phosphate buffer. The region between 450 and 700 nm has been expanded 6-fold.

replaced by a less bulky Ser residue in class III peroxidases and pea cytosolic APX. Consequently, vinyl 2 is less constrained, and two vinyl stretching bands (at about 1620 and 1630 cm^{-1}) are observed in the RR spectra of these proteins (*16*, *18*). Since in KatG the corresponding residue is a threonine (Thr286) (*11*), vinyl 2 can assume an out-of-plane orientation, giving rise to two ν(C═C) bands in the RR spectrum.

Figures 2 and 3 compare the UV−Vis and RR spectra, respectively, of ferric KatG and its variants at pH 7.0. As

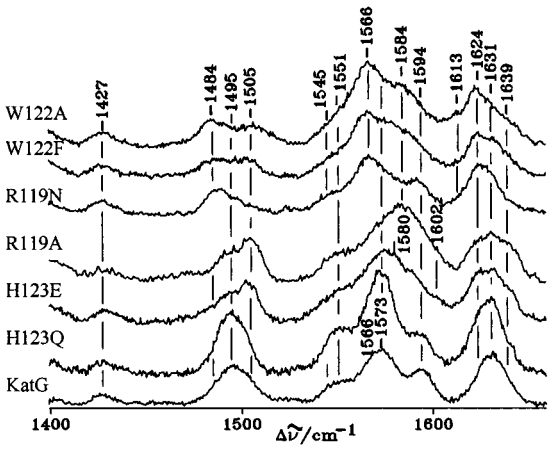

FIGURE 3: RR spectra in the high-frequency region of ferric KatG and the distal mutants H123Q, H123E, R119A, R119N, W122F, and W122A at neutral pH in phosphate buffer obtained with 406.7 nm excitation wavelength. Experimental conditions: 5 cm^{-1} resolution and 15 mW laser power at the sample; (KatG) 16 s/0.5 cm^{-1} collection interval; (H123Q) 17 s/0.5 cm^{-1} collection interval; (H123E) 7 s/0.5 cm^{-1} collection interval; (R119A) 13 s/0.5 cm^{-1} collection interval; (R119N, W122F, and W122A) 9 s/0.5 cm^{-1} collection interval.

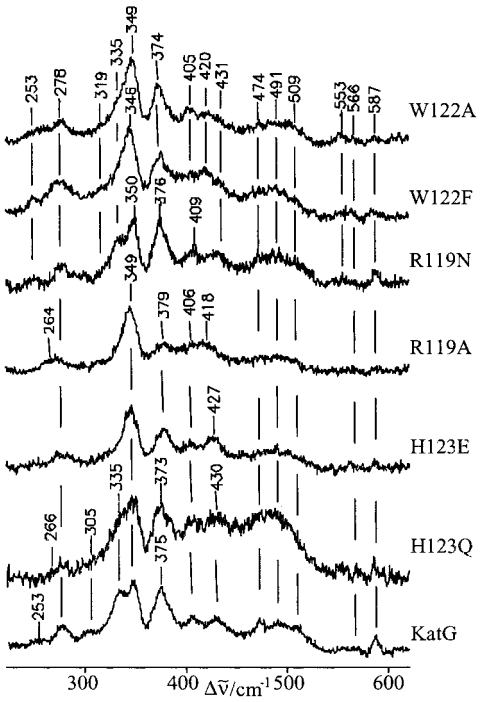

FIGURE 4: RR spectra in the low-frequency region of ferric KatG and the distal mutants H123Q, H123E, R119A, R119N, W122F, and W122A at neutral pH in phosphate buffer obtained with 406.7 nm excitation wavelength. Experimental conditions: 5 cm^{-1} resolution and 15 mW laser power at the sample; (KatG) 9 s/0.5 cm^{-1} collection interval; (H123Q) 15 s/0.5 cm^{-1} collection interval; (H123E) 2 s/0.5 cm^{-1} collection interval; (R119A, W122F, and W122A) 6 s/0.5 cm^{-1} collection interval; (R119N) 7 s/0.5 cm^{-1} collection interval.

previously observed for CCP (*17*, *23*), the single mutation of the key distal residues of KatG alters the coordination and spin states of the heme iron, but no significant changes are observed for the frequencies of the vinyl stretches as compared to wild-type protein (Figure 3). Furthermore, in the present case, the mutants become very unstable and showed an increased tendency to lose the prosthetic heme group. This effect is very pronounced at alkaline pH, and only the H123Q mutant could be titrated. Between pH 10.0 and 11.0, it gives rise to a histidine-iron-hydroxo species (as indicated by the absorption spectrum with bands at 418, 542, and 576 nm) (*23*), coexisting with the free heme (data not shown).

Mutation of the distal His to Gln converts the protein to an almost pure 5-c HS heme as indicated by the blue-shift of the Soret band to 404 nm together with the increase of the shoulder at about 380 nm, the red-shift of the CT1 band to 645 nm, and the RR spectrum mainly characterized by only the core size marker bands of a 5-c HS heme. Quite different is the effect of the His to Glu mutation. In this case, the 5-c HS observed in the wild-type (WT) protein is converted to a 6-c LS heme. In fact, while the CT1 band markedly decreases in intensity, the Soret band red-shifts to 411 nm, and Q-bands are observed at 527 nm and at about 570 nm. Free heme is also present as judged by the shoulder at 368 nm. The weak band at 645 nm is consistent with the weak RR core size marker bands of the 5-c HS heme, whereas the small amount of 6-c HS heme present in the WT protein remains unchanged. The RR spectrum is mainly characteristic of LS heme with core size marker bands at 1505 cm^{-1} (ν_3), at 1580 cm^{-1} (ν_2), at 1602 cm^{-1} (ν_{37}), and at 1639 cm^{-1} (ν_{10}).

Replacement of the distal Arg by Ala gives rise to spectra very similar to those of the H123E mutant. The increase of the shoulder at 368 nm in the UV−Vis spectrum is due to the free prosthetic group, and, consequently, the RR spectrum shows more intense core size marker bands corresponding to the 5-c HS heme than the H123E mutant. The protein is mainly 6-c LS heme (ν_3 at 1505 cm^{-1}, ν_2 at 1584 cm^{-1}, ν_{10} at 1639 cm^{-1}), and the 6-c HS species disappears. Conversely, this latter species becomes dominant in the R119N mutant as suggested by the absence of any shoulder on the blue side of the Soret band which is typical of 5-c HS hemes and confirmed by the RR spectrum (ν_3 at 1484 cm^{-1}, ν_2 at 1566 cm^{-1}, ν_{37} at 1594 cm^{-1}, ν_{10} at 1613 cm^{-1}). A small amount of 6-c LS is also present as indicated by the α band at about 570 nm and the RR ν_3 band at 1505 cm^{-1}.

The substitution of the distal Trp by Phe or Ala gives rise to similar effects, converting the 5-c HS of WT to both 6-c HS and LS hemes. However, a small amount of 5-c HS is still present.

The RR spectra in the low-frequency region (Figure 4) agree well with the conclusions drawn on the basis of the UV−Vis and RR core size marker bands. In particular, following the band assignment obtained for CCP (*22*) and myoglobin (Mb) (*24*) by use of isotopically labeled hemes, the bands of KatG at 335, 349, and 375 nm are assigned to the out-of-plane γ_6, ν_8, and $\delta(C_\beta C_c C_d)$ bending modes of the propionyl substituents of the heme, respectively. The bands at 406 and 430 cm^{-1} are assigned to the $\delta(C_\beta C_a b_d)$ bending modes of the vinyl substituents of the heme. The out-of-plane γ_6 mode at 335 cm^{-1} is enhanced in the 5- and 6-c HS hemes, but disappears in the 6-c LS hemes. Therefore, it cannot be observed in the H123E mutant, and it is very weak in the R119A, W122A, and W122F mutants. As for the high-frequency region, the spectrum of KatG resembles that previously reported for CCP (*17*, *22*). The only notable difference is due to the bending modes of the vinyl groups.

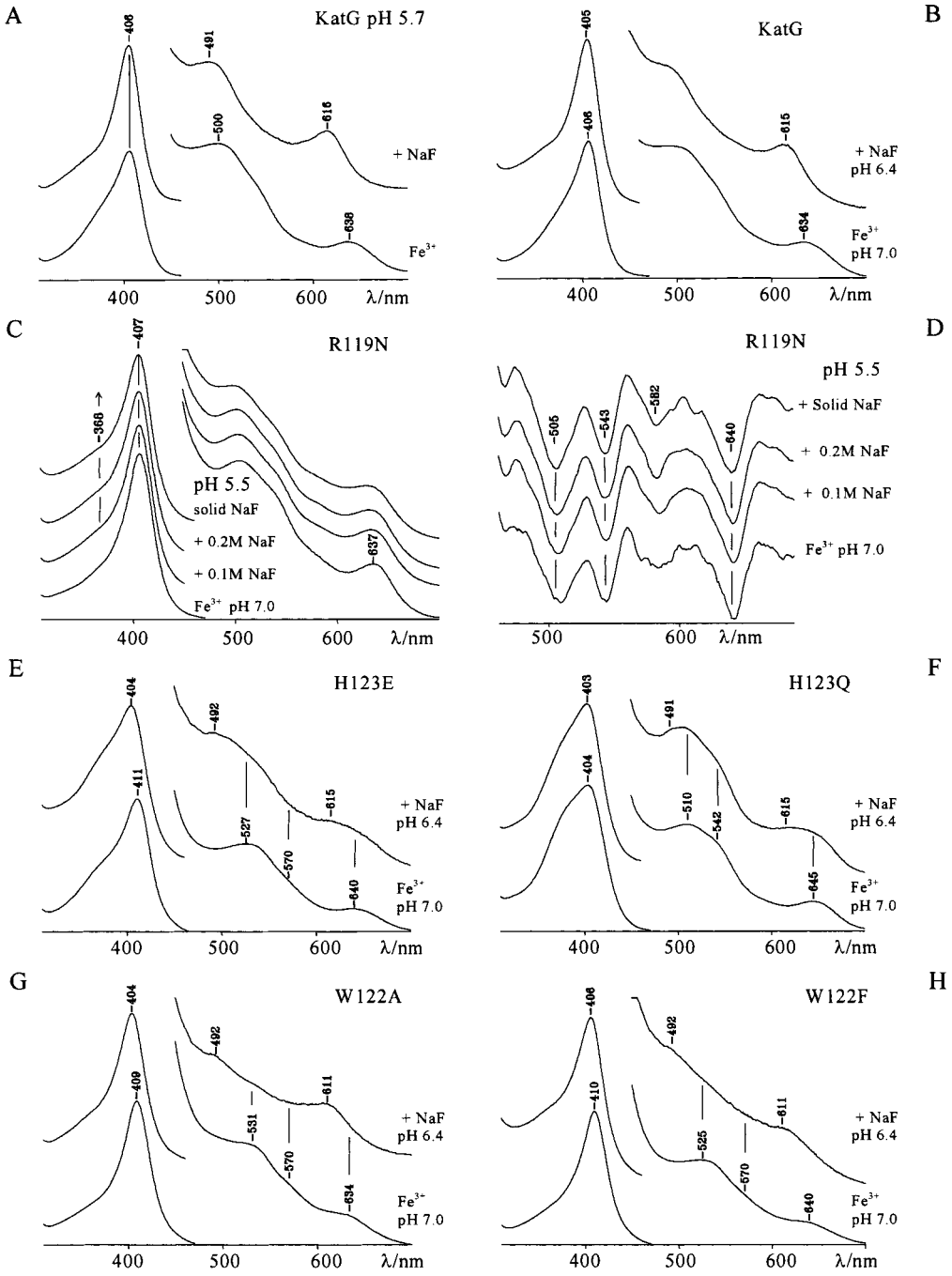

FIGURE 5: Comparison between the electronic absorption spectra of ferric KatG and the distal mutants H123Q, H123E, R119A, R119N, W122F, and W122A and their complex with fluoride. The region between 450 and 700 nm has been expanded 8-fold. (A) KatG at pH 5.7; (B, E−H): bottom spectrum, ferric KatG, H123E, H123Q, W122A, and W122F at pH.7.0; top spectrum, fluoride complexes at pH 6.4; (C) ferric R119N at pH 7.0 and upon increasing concentration of NaF and (D) corresponding second-derivative spectra.

In fact, at neutral pH in CCP, the two vinyl bending modes are coincident and give rise to only one intense band at 406 cm^{-1}.

Fluoride Complexes. The electronic absorption spectrum of the fluoride complex is a sensitive probe of hydrogen bonding interactions between the Fe-bound ligand and distal amino acid residues (*18, 20*). In peroxidases, the distal Arg and His residues are extremely important in stabilizing bound anionic ligands. Furthermore, in class I peroxidases, which contain a distal Trp residue, fluoride is further stabilized by an additional hydrogen bond with this residue. This extra H-bond causes a red-shift of the CT1 band by 4−5 nm with respect to the peroxidases of classes II and III (*18, 20*). Thus, when fluoride acts as a hydrogen bond acceptor, the increase in the number and strength of the hydrogen bonds is manifested by the longer wavelength of the CT1 band (*20*).

The fluoride complex of KatG gives rise to a spectrum similar to that previously obtained for CCP and APX (*18, 20*), with a Soret maximum at 406 nm and a CT1 band at 616 nm (Figure 5A). However, due to the instability of the protein at acidic pH, the fluoride complex of KatG was prepared at a higher pH (pH 5.7) than the optimum pH for fluoride binding (pH 5.0). As a consequence, fluoride is not fully bound, and the presence of unbound protein in the

KatG−F spectrum can be inferred by the broad CT1 band at higher wavelength. A further increase of pH (pH 6.4, Figure 5B) leads to an even great amount of unbound protein.

Figure 5C−H shows the UV−Vis spectra of the mutants upon addition of NaF. The complexes were obtained at pH 6.4 since at lower pH the mutants are very unstable and precipitate. As in CCP (*20*), *Coprinus cinereus* peroxidase (CIP) (*25*), and horseradish peroxidase (HRPC) (*26*), mutation of the distal Arg causes a significant decrease in the affinity for fluoride. This is clearly demonstrated by the absorption spectrum of the R119N mutant which even in excess of fluoride shows the mutant to be in the unligated state (Figure 5C); moreover, the second-derivative spectra do not show any change upon addition of NaF (Figure 5D). As previously reported for CCP (*20*) and HRPC (*26*), without His the fluoride binds very poorly to peroxidases. The UV−Vis spectra of the H123E and H123Q mutants show a high amount of 5-c HS heme due to the noncomplexed protein. However, the absorption maxima of the 6-c HS form (Figure 5E,F) are similar to those of the WT−F adduct. Unlike CCP (*20*), the substitution of the distal Trp with either Ala or Phe affects the ability of the Fe atom to bind fluoride, and an increased unligated species is observed (Figure 5G,H). The CT1 wavelengths in the absorption spectra of the fluoride-ligated proteins are blue-shifted by 4 nm with respect to the parent enzyme as previously observed for the corresponding W51F CCP mutant (*20*), indicating that in KatG the fluoride is hydrogen-bonded to the Trp residue as in CCP and APX (*18*, *20*). The RR spectra of WT and the Trp mutants (data not shown) confirmed the formation of a 6-c HS heme, and, due to the shift of the ν_{10} mode toward lower wavenumbers (1613 cm^{-1}), two vinyl stretches at 1623 and 1631 cm^{-1} were clearly identified.

As in the case of other fluoride complexes with peroxidases, including CCP−F, the ν(Fe−F) stretching mode, whose frequency is sensitive to the hydrogen bonds, is not enhanced via Soret excitation (the only available to us), and the low-frequency RR spectrum of the KatG−F complex is very similar to the unbound ferric protein (data not shown). The RR spectrum is also very similar to that of the CCP−F complex. The only notable difference is the intensity of the bending modes of the vinyl groups observed for the CCP−F adduct at 406 cm^{-1}. This band splits into two bands at 407 and 429 cm^{-1} in the KatG−F adduct as for the ferric protein in the absence of the exogenous ligand.

Ferrous Forms. Figure 6 shows the titration of the reduced protein between pH 5.8 and 9.2. At pH 5.8, the protein is mainly 5-c HS. When the pH is increased, a low-spin heme grows at the expense of the 5-c HS and becomes the most abundant form at pH 9.2. The spectrum of the HS form shows the Soret and the visible maxima (438 and 557 nm) very close to those previously reported for CCP (438 and 559 nm, respectively). The low-spin form shows a Soret maximum at 426 nm, similar to that observed for ferrous CCP at alkaline pH which is due to a bis-imidazole complex (*27*).

The RR spectra in the high-frequency region of ferrous CCP (*17*), KatG, and APX (*18*) are also very similar and characteristic of a 5-c HS heme (data not shown). However, the presence of the 6-c LS heme in KatG is confirmed by the ν_3 mode at 1496 cm^{-1}. The other bands of the LS form are overlapped with those derived from the high-spin form.

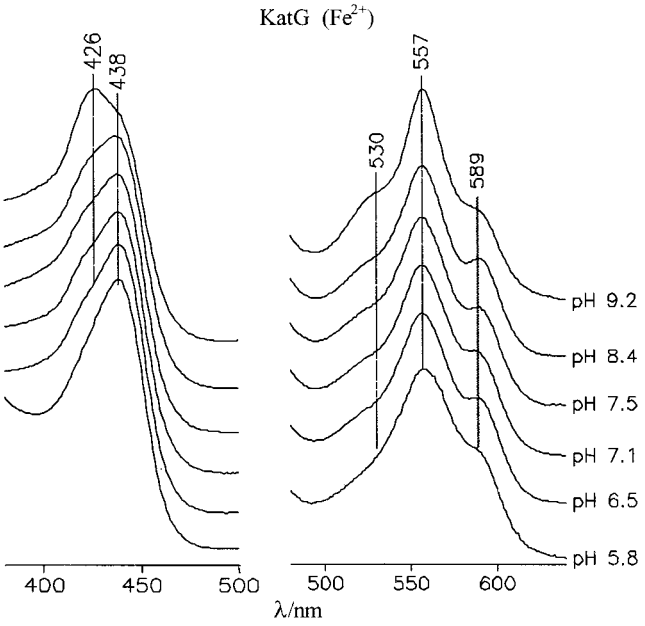

FIGURE 6: Electronic absorption spectra of ferrous KatG at different pH values. The region between 450 and 700 nm has been expanded 5-fold.

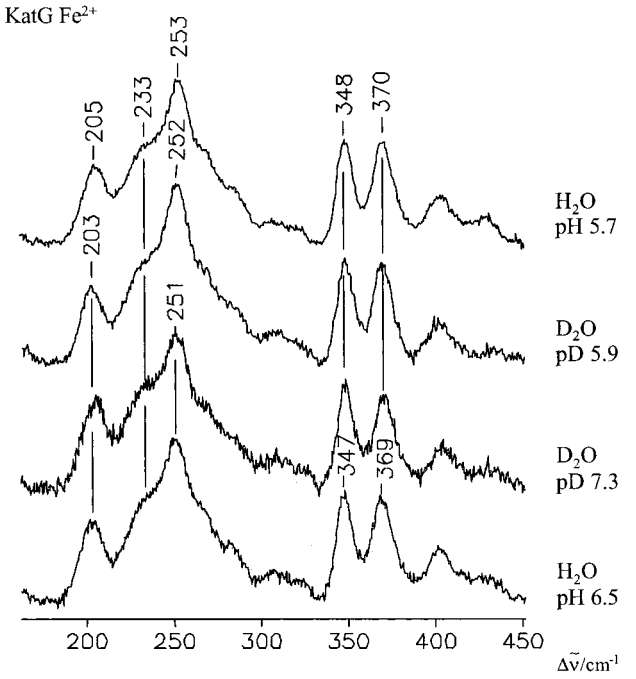

FIGURE 7: RR spectra of ferrous KatG in the low-frequency region in H_2O (pH 5.7 and 6.5) and D_2O (pD 5.9 and 7.3). Experimental conditions: 441.6 nm excitation wavelength, 5 cm^{-1} resolution; (pH 5.7) 30 mW laser power at the sample and 45 s/0.5 cm^{-1} collection interval; (pD 5.9) 25 mW laser power at the sample and 23 s/0.5 cm^{-1} collection interval; (pD 7.3) 25 mW laser power at the sample and 16 s/0.5 cm^{-1} collection interval; (pH 6.5) 20 mW laser power at the sample and 41 s/0.5 cm^{-1} collection interval.

In the vinyl region, the ν(C═C) stretches are observed at 1621 and 1626 cm^{-1}, the former being overlapped with the ν_{10} mode of the 6-c LS heme.

Figure 7 compares the RR spectra in the low-frequency region of KatG taken at pH 5.7 and 6.5, and in deuterated buffers at pD 5.9 and 7.3. The low-frequency region RR spectra of five-coordinate ferrous hemoproteins are characterized by the presence of a strong band due to the iron−

imidazole stretching mode, ν(Fe−Im), which occurs in the region 200−250 cm^{-1}. The hydrogen bond between the N_δ atom of the imidazole fifth ligand and the oxygen atom of the aspartate carboxylate group (characteristic of peroxidases from plants, fungi, and bacteria) gives the proximal ligand imidazolate character and results in both a strengthening of the Fe−imidazole bond and a higher frequency of the associated vibrational mode, as compared to other heme proteins. Therefore, due to its sensitivity to the Fe−Im bond strength, the ν(Fe−Im) stretching mode is a useful probe of the hydrogen bond strength between the conserved proximal histidine and aspartate residues. Moreover, as a consequence of the presence of the hydrogen bond between the proximal histidine and the aspartate, the ν(Fe−Im) stretch is also sensitive to deuteration.

From Figure 7, it can be seen that two bands are sensitive to deuteration and pH: the strong band at 253 cm^{-1}, which downshifts to 252 and 251 cm^{-1} in D_2O and at pH 6.5, respectively, and the band at 205 cm^{-1}, which downshifts to 203 cm^{-1} in both higher pH and D_2O. Raising the pH of reduced KatG from 7.3 to 8.2 caused no observable shift of any band in the region (data not shown). In analogy with the similar results obtained for ferrous CCP (*22*) and APX (*18*), we assign these two bands to two ν(Fe−Im) stretching modes which are distinguished by the strength of the hydrogen bond between the proximal His and the Asp carboxylate side chain. The band at 205 cm^{-1} should correspond to a species whose proton resides on the imidazole, while in the other the proton is transferred to the carboxylate. As in APX, the absence of a decrease of the I_{205}/I_{253} intensity ratio between the two bands, going from lower to higher pH, suggests that the two species are independent and not in equilibrium as in CCP or CIP (*22, 28*). Moreover, the shift of frequency of the ν(Fe−Im) stretches in KatG is observed at about 2 pH units lower than in CCP and APX, but very similar to that observed for lignin peroxidase (LIP) (found at about pH 5.0, unpublished data).

The pH titration of the mutants in their reduced form resembles that of the WT protein (data not shown). The mutants were very unstable at pH lower than 6.5, and the amount of the 6-c LS heme is higher in the mutants than in the wild-type protein even at pH 6.5 (Figure 8). This species increases at higher pH, as suggested by an increase in intensity of the lower wavelength component of the Soret band (423 nm), a concomitant decrease of the maximum at 439 nm, and the increase of the band at 531 nm (data not shown). At pH 6.5, the spectrum of the R119A mutant is an almost complete 6-c LS heme, as indicated by the Soret band at 423 nm, and the Q-bands at 531 and 557 nm. The weak shoulders observed at 439 and 587 nm are due to the contribution of the small amount of 5-c HS heme which is still present. The H123Q and R119N mutants are converted to an almost pure 6-c LS heme at pH 9.8 and 9.0, respectively, a value lower than that of the WT protein (see Figure 6) (data not shown).

Figure 9 shows the RR spectra of the reduced forms of the mutants in the low-frequency region at pH 6.5. The spectrum of KatG is also reported for comparison. The two ν(Fe−Im) stretches, observed at 251 and 203 cm^{-1} in the parent enzyme, shift to lower frequency in the H123Q, H123E, and R119N mutants, indicating that distal mutation

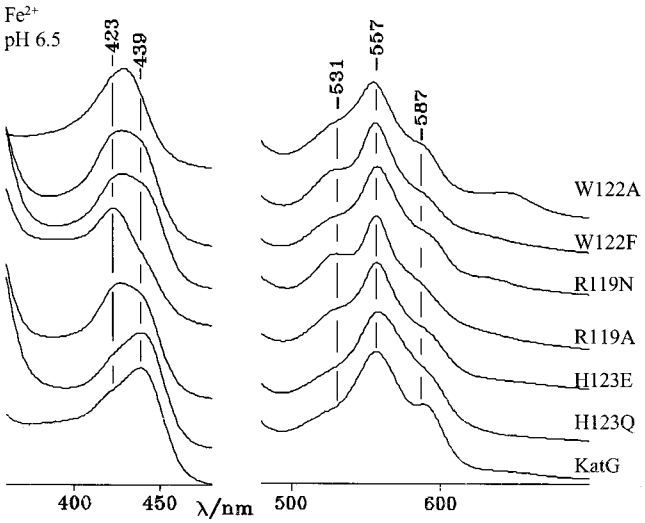

FIGURE 8: Electronic absorption spectra of ferrous KatG and the distal mutants H123Q, H123E, R119A, R119N, W122F, and W122A at pH 6.5. The region between 450 and 700 nm has been expanded 5-fold.

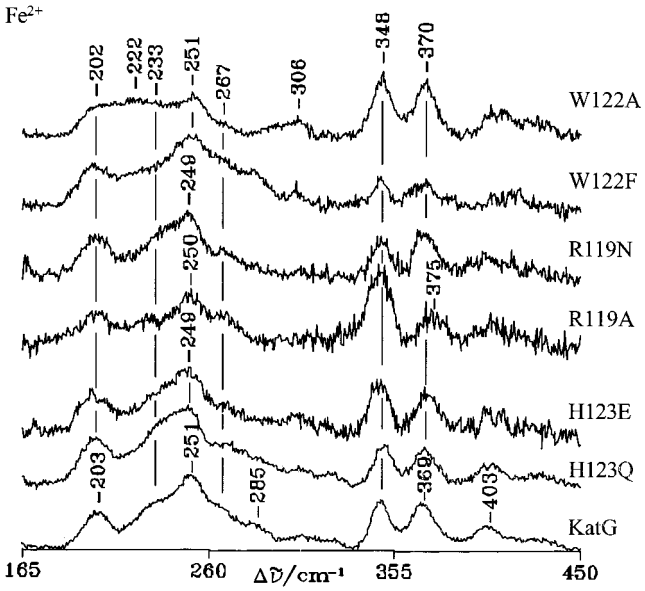

FIGURE 9: RR spectra of ferrous KatG in the low-frequency region and the distal mutants H123Q, H123E, R119A, R119N, W122F, and W122A at pH 6.5. Experimental conditions: 441.6 nm excitation wavelength, 20 mW (KatG) 30 mW (distal mutants) laser power at the sample, 5 cm^{-1} resolution; (KatG) 41 s/0.5 cm^{-1} collection interval; (H123Q) 6 s/0.5 cm^{-1} collection interval; (H123E) 18 s/0.5 cm^{-1} collection interval; (R119A) 9 s/0.5 cm^{-1} collection interval; (R119N) 9 s/0.5 cm^{-1} collection interval; (W122F) 12 s/0.5 cm^{-1} collection interval; (W122A) 18 s/0.5 cm^{-1} collection interval.

has weakened the proximal hydrogen bond. This was previously observed in the corresponding mutants of CCP (*17, 23*), CIP (*25*), and HRPC (*26, 29*), and confirms that also in KatG there is connection between the distal and proximal sides of the heme cavity. No clear conclusion can be drawn for the R119A mutant since the spectrum derives from the overlapping contribution of the bands of both HS and LS hemes, the latter being the major component. The changes observed in the spectrum of the W122A are quite intriguing. In this case, as for the W122F, the mutation does not affect the frequency of the Fe−Im stretching mode. However, an intensity increase of a band at 222 cm^{-1} is

observed. This band is not sensitive to deuteration (data not shown) and could be due to a porphyrin mode present in this region. It is not clear why it is enhanced upon mutation. It must be noted that also the band at 306 cm^{-1} appears stronger in the W122A spectrum as compared to the other proteins.

DISCUSSION

KatG shares many common characteristics with both CCP and APX, but some differences can be inferred, mainly on the basis of the effects induced upon distal mutation. Moreover, KatG from *Synechocystis*, although very similar to that from *Mycobacterium tuberculosis*, shows interesting peculiarities.

Coordination and Spin States. At neutral pH, ferric KatG is mainly 5-c HS. Small amounts of both 6-c HS and 6-c LS are observed. The spectrum is very similar to that of CCP, but with a higher proportion of the 6-coordinate species. The 6-c HS heme is probably due to a water molecule bound to the heme iron. More uncertain is the nature of the sixth ligand giving rise to the LS form. Based on previous results, two ligands are usually found to be coordinated to the sixth position of the heme iron in the low-spin species: the distal His or a hydroxo group. The UV−Vis spectra of these two types of 6-c LS hemes are distinctly different. A bis-His-type spectrum closely matches that of ferric cytochrome b_5 with the Q-bands at about 560 (α band) and 530 (β band) nm, the former being a shoulder. The 6-c LS heme with a hydroxide as sixth ligand resembles those of alkaline Mb, HRPC, and CIP, with two well-separated Q-bands around 575 and 545 nm (*23*, *30*, *31*). In the present case, no conclusions can be drawn on the nature of the sixth ligand at neutral pH, since the amount of low-spin is too low to give rise to reasonably intense Q-bands. On the other hand, the alkaline transition could not be observed since the protein is very unstable at pH higher than 9.5 and loses heme before the alkaline transition is detected.

At neutral pH, APX is predominantly a high-spin five-coordinate histidine-ligated enzyme (like that of CCP), with contributions from six-coordinate high- and low-spin complexes that are histidine-aquo, histidine-hydroxide, and bis-histidine (*18*, *32*). A similar set of coordination states appears probable also for KatG. However, mutation of the distal residues causes a decrease of the pK_a of the alkaline transition, and the H123E, R119A, W122F, and W122A mutants show an increased amount of low spin at neutral pH. The band at 570 nm observed in the electronic absorption spectra suggests either a water molecule with some OH^- character (i.e., strongly hydrogen bonded) or a pure hydroxo ligand bound to the heme iron. Accordingly, in the alkaline form of the H123Q mutant, the formation of a histidine-iron-hydroxo species was clearly observed. Moreover, the virtual disappearance of the 6-c LS heme upon fluoride binding in the wild-type KatG indicates that the internal ligand could be displaced by the fluoride, and, therefore, confirms that it can be assigned to a hydroxo-type ligand.

The only other catalase-peroxidase that has been fully characterized by optical and RR spectroscopy is that from *Mycobacterium tuberculosis* (*33*), which is slightly different from that of *Synechocystis*. The optical and RR spectra indicate that the protein is a mixture of HS and LS hemes, as the one from *Synechocystis*, but the amount of LS is higher than that observed for the present case and remains clearly evident upon addition of fluoride at pH 5.3. The LS heme increased at low temperature, and EPR data are consistent with an endogenous strong-field sixth ligand (3.24, 2.05, 1.28). However, comparison with the data obtained on the S315T mutant showed that mutation increases the amount of low spin at room temperature, but the corresponding low-temperature EPR spectra are characterized by a lower g_{max} (2.48, 2.28, 1.88) than observed for the wild-type protein. The authors conclude that the mutant is consistent with a bis-imidazole complex where one or both histidines are deprotonated and suggest as probable candidate the distal imidazole of His108. However, the similarity of the *g* values to those reported for Mb at alkaline pH (2.55, 2.17, 1.85) or other model compounds (*34*) which bind a hydroxo ligand in the distal iron coordination raises the possibility of an His-OH^- axial coordination. The nature of the sixth ligand in the wild-type remains unclear. In fact, the large g_{max} EPR leaves some questions concerning the identity of the endogenous distal ligand. If this residue is the distal His, as it is supposed to be for the mutant, the EPR spectrum indicates that its geometry is very different from that of the mutant and the two imidazole planes are nearly mutually orthogonal (*35*). The EPR spectrum is, in fact, very similar to that of HRPA2 at pH 7.5 or upon addition of imidazole (*36*), suggesting that the KatG from *Mycobacterium tuberculosis* has a bis-His coordination. In the present case, a detailed analysis of the optical, RR, and EPR spectra at low temperatures is necessary to establish the nature of the sixth ligand giving rise to a 6-c LS heme. Interestingly, ferrous KatG from *Synechocystis* at acidic pH is mainly 5-c HS heme with optical spectra very similar to the other peroxidases of class I, but already at pH 6.5 a low-spin form appears which increases upon increasing the pH. This form is characterized by a Soret maximum at about 425 nm and bands in the visible region with maxima at about 530 and 557 nm. The spectrum is very similar to those of alkaline CCP and ferrous cytochrome b_5, which are known to be six-coordinate bis-histidine-ligated species. The interpretation of these results becomes very intriguing considering that the amount of low spin increases in the mutants including the H123E and H123Q proteins. This form appears to be connected with the loss of the heme prosthetic group. The amount of LS heme is very high in the R119A and H123E mutants which show also a high amount of free heme in their ferric form. Moreover, it increases at higher pH, where the proteins lose the prosthetic groups very easily in their ferric forms. Interestingly, upon complexation with CO, the ν(CO) frequencies are characteristic of an "open cavity" (data not shown). Therefore, the LS form might derive from another distal residue, apart from the distal His, capable of coordinating the heme iron as a consequence of a partial unfolding of the protein.

Heme Distal Cavity. The effects of distal mutation on the stability of the heme architecture and on the Fe coordination and spin states of KatG suggest the following conclusions:

First, KatG is less stable than other peroxidases, and the charge and the steric hindrance of the distal residues appear particularly important for maintaining the heme architecture. The R119A mutant is particularly unstable, easily losing the prosthetic group even at neutral pH. This is unusual since

the replacement of the distal Arg with the nonpolar residue Leu in CCP (*23*), HRPC (*26*), and CIP (*25*) gave rise to the formation of an almost pure high-spin five-coordinate histidine-ligated enzyme, whereas the substitution of Arg by Gly in HRPC gave rise to the formation of an aquo 6-c HS species (*26*). Likewise, the H123E KatG mutant loses heme at neutral pH while the corresponding HRPC mutant, H42E, is mainly 6-c HS heme (*26*). These data allow us to conclude that a negatively charged residue in the distal cavity destabilizes the heme pocket. Moreover, the results suggest that a weaker binding of the heme might derive from changes in the protein structure resulting from loss of H-bonding and/or salt bridges**.** Interestingly, the electronic absorption maxima reported for the Arg to Leu mutant of the hydroperoxidase I KatG from *E. coli* suggest the presence of a 5-c HS species (*12*) as for the other peroxidases reported above. Some changes in the coordination and spin state can also be inferred by the absorption maxima reported in the Table for various distal mutations (*12*), but in the absence of a visual inspection of the spectra, any firm conclusion is very difficult. In the same paper, the authors report that distal mutants of KatG from *E. coli* bind the heme group very poorly.

Second, the substitution of the distal Arg with an asparagine residue causes the formation of an aquo 6-c HS species, as previously found for the R51N CIP mutant (*25*). Therefore, these results clearly indicate the presence of a hydrogen bond network involving water molecules and the polar residues in the distal cavity. The substitution of the positively charged guanidinium group with a neutral amide group destabilizes the hydrogen bond network with the water molecules, allowing a distal water molecule to bind the iron atom.

Third, the substitution of the distal Trp either with Ala or with Phe gives rise to very similar results. First of all, mutation caused a marked decrease of the pK_a of the alkaline transition, and a low-spin species appears at neutral pH. Moreover, as for the corresponding W51F CCP mutant (*7*), the formation of a 6-c HS heme with a water molecule coordinated to the heme iron is observed. This confirms the presence of water molecules in the distal cavity involved in a H-bond network with the amino acid residues and that the distal Trp appears to be directly involved in this network, as found for CCP and APX. The replacement of the hydrogen bond donor indole group of Trp by a non-H-bonding residue allows the distal water molecule to bind the heme iron.

And, fourth, KatG binds fluoride in the same way as CCP and APX, and the fluoride anion, bound to the heme Fe atom, is stabilized by three hydrogen bonds: probably with Arg119, a water molecule bridged with the distal His123, and Trp122.

Proximal Heme Cavity. Two independent ν(Fe−Im) stretches were found in KatG as in APX (*18*), but only the low-frequency band (205 cm^{-1}) matches one of those of APX, whereas the other has a fairly high-frequency resembling CCP (*22*). Moreover, for KatG the pK_a of the acid−alkaline form appears to be particularly low and very similar to that of LIP (unpublished results). Distal mutation alters the proximal Fe−Im strength. In particular, the replacement of both the distal His and Arg causes a downshift of the frequency of the intense ν(Fe−Im) stretching mode at higher frequency with respect to the wild-type protein. Therefore, one may infer, as previously found for CCP (*17, 23*), CIP (*25*), and HRPC (*26, 29*), that mutation of the distal Arg and His key residues weakens the hydrogen bond between the proximal histidine and aspartate residues, reflecting a more neutral, less imidazolate character, of the axial ligand. These effects probably result from perturbation of a hydrogen-bonding network extending between the distal and proximal sides of the heme, as a consequence of the distal mutations. As for the W51F CCP mutant (*17*) or the Phe mutants of HRPC (*29*) and CIP (*37*), no alterations on the proximal side were caused by the replacement of the distal Trp in KatG.

Ferrous KatG from *Mycobacterium tuberculosis* behaves similarly to our protein in terms of the high-spin−low-spin equilibrium upon titration. However, the two ν(Fe−Im) stretches identified at 244 and 228 cm^{-1} are pH-dependent (*33*). The band at 244 cm^{-1} is very strong at pH 8.0, and a weak shoulder at 228 cm^{-1} appears at pH 10.0. The behavior and the frequencies of the Fe−Im stretches resemble very closely those of CCP, where the two bands arise from two tautomers of the hydrogen bond between the proximal His and an aspartic carboxylate side chain. The comparison of these results with the present data obtained for *Synechocystis* KatG suggests some differences in the proximal side of these two catalase-peroxidases which are not obvious from sequence alignment and secondary structure prediction (*11*).

Vinyl Orientation. Two ν(C═C) vinyl stretches are found with frequencies very similar to those observed in APX. These data suggest that the vinyl orientation is similar to that of APX and show the importance of the nature of the residues near the vinyl groups. In CCP, the Met172 side chain is found in close proximity to vinyl 2, whereas in APX the corresponding residue is Ser160, which causes less steric hindrance allowing a free orientation of vinyl 2 (1629 cm^{-1} instead of 1618 cm^{-1} as in CCP). In *Synechocystis* KatG, the corresponding residue is a threonine (Thr286), and, therefore, two vinyl stretches can be expected. Interestingly, in the KatG from *Mycobacterium tuberculosis*, which contains an Ile in the corresponding position, the orientation of the vinyl substituents appears different since only one ν(C═C) at 1623 cm^{-1} and two bending modes at 403 and 418 cm^{-1} have been identified (*33*). Vinyl 2 appears to be sterically hindered by the Ile and, therefore, is forced to change its orientation. A similar situation is found for CIP in which the steric hindrance of a Leu residue leads to two overlapping ν(C═C) stretches at 1625 cm^{-1} (*31*). Moreover, the vinyl orientation is not changed by distal mutation, including W122A and W122F, suggesting that these distal residues are not in close proximity to the vinyl substituents and do not contribute to their orientation, in contrast to the corresponding position of CIP (*37*).

Structure−Function Relationship. From the present data, we can conclude that the distal cavity of KatG is very similar to that of the other class I peroxidases. A H-bond network is present, involving water molecules, Trp, His, and Arg residues, which connect the proximal and distal sides of the heme pocket. Mutations of the key distal residues Arg and His perturb the proximal Fe−Im bond strength, resulting in a weakening of the H-bond between the proximal histidine and aspartate residues. It is interesting that mutation of the distal Trp does not influence the H-bonding network at the proximal side. However, the formation of a histidine−hydroxide low-spin heme complex at neutral pH in both the W122A and W122F mutants, together with the important

role played by the Trp residue in fluoride binding, indicates the significant role of this residue in distal H-bonding. This role appears much more pronounced than in CCP, where the Trp51 to Phe mutation leaves unaltered not only the proximal Fe−Im strength and the ability of fluoride binding but also the spin state: the mutant remains in a high-spin state (*17*, *20*). Certainly, the formation of the low-spin state at neutral pH in the KatG Trp mutants can easily explain why the reaction rate between these mutants and hydrogen peroxide was found to be about 2 orders of magnitude lower relative to the value of $k_{1(app)}$ of a typical peroxidase (*13*). This behavior contrasts with that of the W51F CCP variant for which the bimolecular rate constant of compound I formation is relatively unaffected as compared to the parent enzyme. These findings might be of relevance for the catalase activity of KatG since mutation of the distal Trp strongly influences compound I reduction by H_2O_2. The *Synechocystis* enzyme completely lost its catalase activity in the Trp variants, underlining the important role of the indole moiety in distal H-bonding and binding and orientation of the second hydrogen peroxide molecule (*13)*. Moreover, we have recently shown that the W122F variant completely lost its chlorination and bromination reactivity normally observed with wild-type *Synechocystis* KatG (*38*), indicating that generally halide binding could occur in the same way as demonstrated for fluoride. By contrast, mutation of the distal amino acids had no effect on compound I reduction by typical aromatic one-electron donors (*14*). This indicates that—similar to other peroxidases—the binding site of typical peroxidase substrates could be at the δ-meso carbon of the heme (*39*) and is not influenced by perturbation of the H-bonding pattern upon replacement of distal Arg, Trp, or His.

It is also worth noting that the reduction potential of the ferric/ferrous couple in catalase-peroxidases could be much more positive compared to other members of peroxidase superfamily I. Recently, a midpoint potential of −50 mV was published for *Mycobacterium tuberculosis* KatG (*40*). Although this cannot necessarily be extrapolated to the catalytic intermediates of KatG, the finding that chloride can be oxidized (*38*) provides evidence that the reduction potential of the couple compound I/native enzyme is also higher than that of other members of peroxidase superfamily I. An important factor that strongly influences the redox potential of Fe is the imidazolate character of the proximal histidine, which is determined by the strength of the H-bond between the N_δ atom of the imidazole fifth ligand and the oxygen of the aspartate carboxylate group. This was impressively shown for wild-type CCP [$E°'(Fe^{3+}/Fe^{2+}) = -183$ mV] and the D235N variant [$E°'(Fe^{3+}/Fe^{2+}) = -79$ mV] (*41*). The higher redox potential of KatGs suggests a more neutral, less imidazolate character, which is also indicated by the RR spectra obtained in this work. The structural basis for this findings could be that KatGs contain conserved insertions on the proximal heme side which could totally reconstruct the proximal heme side compared to APX and CCP and thus modulate the Fe-imidazole coordination (*11*). The secondary structure prediction in the region of the proximal His reveals different structure arrangements for KatGs compared to APX and CCP. Whereas the proximal His in APX and CCP is known to be located in a truncated α-helix (*8*, *9*), in KatGs the corresponding His is located on the edge of an extended β-structure. The location of the proximal Asp of KatG is predicted to be between the third KatG-specific insertion and helix H (*11*), in contrast to its location in helix H in APX. On one hand, this influences the relative position, distance, and basic character of the proximal His, and contributes to the reduction potential and as a consequence to the thermodynamic capability of KatG to oxidize chloride. On the other hand, the Trp involved in the pronounced H-bonding pattern at the distal side seems to provide the optimal binding conditions for anions and the second H_2O_2 molecule necessary for the catalase reaction.

REFERENCES

1. Welinder, K. G. (1992) *Curr. Opin. Struct. Biol. 2*, 388−393.
2. Mutsuda, M., Ishikawa, T., Takeda, T., and Shigeoka, S. (1996) *Biochem. J. 316*, 251−257.
3. Nagy, J. M., Cass, A. E. G., and Brown, K. A. (1997) *J. Biol. Chem. 272*, 31265−31271.
4. Johnsson, K., Frol, W. A., and Schultz, P. G. (1997) *J. Biol. Chem. 272*, 2834−2840.
5. Forkl, H., Vandekerckhove, J., Drews, G., and Tadros, M. H. (1993) *Eur. J. Biochem. 214*, 251−258.
6. Jakopitsch, C., Rüker, F., Regelsberger, G., Dockal, M., Peschek, G. A., and Obinger, C. (1999) *Biol. Chem. Hoppe-Seyler 380*, 1987−1996.
7. Engleder, M., Regelsberger, G., Jakopitsch, C., Furtmüller, P. G., Rüker, F., Peschek, G. A., and Obinger, C. (2000) *Biochimie 82*, 211−219.
8. Finzel, B. C., Poulos, T. L., and Kraut, J. (1984) *J. Biol. Chem. 259*, 13027−13036.
9. Patterson, W. R., Poulos, T. L., and Goodin, D. B. (1995) *Biochemistry 34*, 4342−4345.
10. Zámocký, M., Janecek, Š., and Koller, F. (2000) *Gene 256*, 169−182.
11. Zámocký, M., Regelsberger, G., Jakopitsch, C., and Obinger, C. (2001) *FEBS Lett. 492*, 177−182.
12. Hillar, A., Peters, B., Pauls, R., Loboda, A., Zhang, H., Mauk, A. G., and Loewen, P. C. (2000) *Biochemistry 39*, 5868−5875.
13. Regelsberger, G., Jakopitsch, C., Rüker, F., Krois, D., Peschek, G. A., and Obinger, C. (2000) *J. Biol. Chem. 275*, 22854−22861.
14. Regelsberger, G., Jakopitsch, C., Rüker, F., Switala, J., Loewen, P., and Obinger, C. (2001) *Biochem. Soc. Trans. 29*, 99−105.
15. Rouse, D. A., DeVito, J. A., Li, Z., Byer, H., and Morris, S. L. (1996) *Mol. Microbiol. 22*, 583−592.
16. Smulevich, G. (1998) *Biospectroscopy 4*, S3−17.
17. Smulevich, G., Mauro, J. M., Fishel, L. A., English, A. M., Kraut, J., and Spiro, T. G. (1988) *Biochemistry 27*, 5477−5485.
18. Nissum, M., Neri, F., Mandelman, D., Poulos, T. L., and Smulevich, G. (1998) *Biochemistry 37*, 8080−8087.
19. Kalsbeck, W. A., Robertson, D. E., Pandey, R. K., Smith, K. M., Dutton, P. L., and Bocian, D. F. (1996) *Biochemistry 19*, 3429−3438.
20. Neri, F., Kok, D., Miller, M. A., and Smulevich, G. (1997) *Biochemistry 36*, 8947−8953.
21. Wang, J. M., Mauro, M., Edwards, S. L., Oatley, S. J., Fishel, L. A., Ashford, V. A., Xuong, N. H., and Kraut, J. (1990) *Biochemistry 29*, 7160−7173.
22. Smulevich, G., Hu, S., Rodgers, K. R., Goodin, D. B., Smith, K. M., and Spiro, T. G. (1996) *Biospectroscopy 2*, 365−376.
23. Smulevich, G., Miller, M. A., Kraut, J., and Spiro, T. G. (1991) *Biochemistry 30*, 9546−9558.
24. Hu, S., Smith, K. M., and Spiro, T. G. (1996) *J. Am. Chem. Soc. 118*, 12638−12646.
25. Neri, F., Indiani, C., Welinder, K. G., and Smulevich G. (1998) *Eur. J. Biochem. 251*, 830−838.
26. Howes, B. D., Rodriguez-Lopez, J. N., Smith, A. T., and Smulevich, G. (1997) *Biochemistry 36*, 1532−1543.
27. Smulevich, G., Miller, M. A., Gosztola, D., and Spiro, T. G. (1989) *Biochemistry 28*, 9905−9908.
28. Smulevich, G., Feis, A., Focardi, C., Tams, J., and Welinder, K. G. (1994) *Biochemistry 33*, 15425−15432.
29. Smulevich, G., Paoli, M., Burke, J. F., Sanders, S. A., Thorneley, R. N. F., and Smith, A. T. (1994) *Biochemistry 33*, 7398−7407.
30. Feis, A., Marzocchi, M. P., Paoli, M., and Smulevich, G. (1994) *Biochemistry 33*, 4577−4583.

31. Smulevich, G., Neri, F., Marzocchi, M. P., and Welinder, K. G. (1996) *Biochemistry 35*, 10576−10585.
32. Cheek, J., Mandelman, D., Poulos, T. L., and Dawson, J. H. (1999) *J. Biol. Inorg. Chem. 1*, 64−72.
33. Lukat-Rodgers, G. S., Wengenack, N. L., Rusnak, F., and Rodgers, K. R. (2000) *Biochemistry 39*, 9984−9993.
34. Kraus, D. W., Wittenberg, J. B., Jing-Fen, L., and Peisach, J. (1990) *J. Biol. Chem. 265*, 16054−16059.
35. Walker, F. A. (1999) *Coord. Chem. Rev. 185*−*186*, 471−534.
36. Howes, B. D., Feis, A., Indiani, C., Marzocchi, M. P., and Smulevich, G. (2000) *J. Biol. Inorg. Chem. 5*, 227−235.
37. Neri, F., Indiani, C., Baldi, B., Vind, J., Welinder, K. G., and Smulevich, G. (1999) *Biochemistry 38*, 7819−7827.
38. Jakopitsch, C., Regelsberger, G., Furtmüller, P. G., Rüker, F., Peschek, G. A., and Obinger, C. (2001) *Biochem. Biophys. Res. Commun. 287*, 682−687.
39. Ator, M. A., David, S. K., and Ortiz de Montellano, P. R. (1987) *J. Biol. Chem. 262*, 14954−14960.
40. Wengenack, N. L., Lopes, H., Kennedy, M. J., Tavares, P., Pereira, A. S., Moura, I., Moura, J. G., and Rusnak, F. (2000) *Biochemistry 39*, 11508−11513.
41. Goodin, D. B., and McRee, D. E. (1993) *Biochemistry 32*, 3313−3324.

BI025740U